Stable Walking of a 7-DOF Biped Robot

Franck Plestan, *Associate Member, IEEE*, Jessy W. Grizzle, *Fellow, IEEE*, Eric R. Westervelt, *Student Member, IEEE*, and Gabriel Abba, *Member, IEEE*

***Abstract*—The primary goal of this paper is to demonstrate a means to prove asymptotically stable walking in an underactuated, planar, five-link biped robot model. The analysis assumes a rigid contact model when the swing leg impacts the ground and an instantaneous double support phase. The specific robot model analyzed corresponds to a prototype under development by the Centre National de la Recherche Scientifique (CNRS), Paris, France. A secondary goal of the paper is to establish the viability of the theoretically motivated control law. This is explored in a number of ways. First, it is shown how known time trajectories, such as those determined on the basis of walking with minimal energy consumption, can be incorporated into the proposed controller structure. Secondly, various perturbations to the walking motion are introduced to verify disturbance rejection capability. Finally, the controller is demonstrated on a detailed simulator for the prototype which includes torque limits and a compliant model of the walking surface, and thus a noninstantaneous double support phase.**

***Index Terms*—Biped robot, optimal trajectories, Poincaré sections, rigid and compliant contact models, robustness evaluation, stable walking.**

I. Introduction

DURING the two last decades, the interest in legged robots has increased and has even given rise to a few spectacular products, like Honda's humanoid robot,[1] and Sony's dog-like and bipedal robots.[2] Good surveys can be found in [36], [40], [44], and [46] and a large database of walking robots is available at http://www.uwe.ac.uk/clawar/. Representative papers in the more recent literature on controlled, bipedal robots include [11], [19], [27], [33], [34], [47], [49]. Bipedal robots are being controlled to walk, jump, and run. With very few exceptions, the determination of whether a control law applied to a legged robot yields a "stable" walking or running motion has been based on extensive simulations or on building the robot and implementing the control law. In this sense, theory is significantly trailing practice.

Manuscript received March 19, 2002; revised September 23, 2002. This paper was recommended for publication by Associate Editor M. Buehler and Editor A. De Luca upon evaluation of the reviewers' comments. The work of J. W. Grizzle and E. Westervelt was supported in part by the National Science Foundation under Grant INT-9980227 and under Grant IIS-9988695, and in part by the University of Michigan Center for Biomedical Engineering Research (CBER).

F. Plestan is with the IRCCyN, Ecole Centrale de Nantes, 44321 Nantes Cedex 03, France (e-mail: Franck.Plestan@irccyn.ec-nantes.fr).

J. W. Grizzle and E. R. Westervelt are with the Control Systems Laboratory, Electrical Engineering and Computer Science Department, University of Michigan, Ann Arbor, MI 48109-2122 USA (e-mail: grizzle@umich.edu; ewesterv@umich.edu).

G. Abba is with the LGIPM, Université de Metz, 57970 Yutz, France (e-mail: abba@iut.univ-metz.fr).

Digital Object Identifier 10.1109/TRA.2003.814514

As may be expected, the greatest analytical progress on stability analysis has been in the case of fully actuated robots (an actuator for each mechanical degree of freedom). A key aspect of [42] is that a periodic orbit is created without tracking a pre-computed trajectory, leading to a time-invariant closed-loop system for which stability has been analyzed. For under actuated robots, which is the topic of this paper, a rather complete stability analysis has been achieved in two main cases: the biped compass model without a torso [13], [45] (an extended model with a torso locked at right angle to the walking surface has been analyzed in [17]) and the monopod hopper of Raibert [39]. The stability analysis of the compass model is based on numerically computing the Poincaré map, determining a fixed point through a Newton-Raphson search, and then linearizing about the fixed point [32]. The numerical difficulty in checking stability in this manner increases rapidly with the dimension of the model. In the case of the hopper, analytical progress was based on deriving approximate models of the hopper for which the associated Poincaré return map can be computed in closed-form [10], [23], [41]. This in turn has led to the determination of sampled-data control laws (sampling is done synchronously with impact events) that admit low-dimensional tests for asymptotic stability of a periodic orbit. Bipeds are much more complex than the hopper. Even for a stiff-legged biped model with a torso, determining a closed-form representation of the Poincaré return map would be a formidable task (essentially a map from $\mathbb{R}^5$ to itself), and doing this for the case of a robot with knees is simply unthinkable at the present time (a map from $\mathbb{R}^9$ to itself, or worse). Indeed, the complexity of the equations of motions has been used as a justification for intuitive control methods;[3] see [35].

The control work closest in spirit to that presented here is [30]. As in [42], this innovative paper also focuses on achieving walking motions in a robot without recourse to a pre-computed set of reference trajectories. The studied robot is planar and under actuated, consisting of two legs without feet connected at a hip; there is no torso. The legs have revolute knees that are unactuated, but which are equipped with blocks so that they lock in the extended position before impact. Consequently, the stability analysis is similar to that of the compass model. A single actuator is provided at the hips, exerting a torque between the two femurs. The control law is parameterized in terms of the absolute angle of the swing leg tibia. Stability is investigated by numerically computing the Poincaré map and evaluating its eigenvalues about a fixed point. The control law was also implemented experimentally. Once the mass and inertial parameters of the analytical model were identified from the experimental robot and joint friction was estimated, the experiments

[1][Online.] Available: http://www.honda.co.jp/robot/

[2][Online.] Available: http://www.sony.co.jp/en/Products

[3][Online.] Available: http://www.ai.mit.edu/projects/leglab/

coincided very well with the theory. A similar set of results for the giant swing motion of a gymnastic robot is presented in [31].

The main objective of this paper is to propose, for an under actuated bipedal robot with a torso and revolute knees, but no feet, a novel and complete asymptotic stability proof for a periodic walking motion on a rigid, flat surface. The key breakthrough behind this is the development in [14] of a continuous-time control strategy and a novel extension of Poincaré's method that significantly reduce the dimension of the stability analysis problem: for a class of hybrid, mechanical systems with N degrees of freedom (DOF) and $(N-1)$ independent actuators, the stability analysis problem is formally reduced to the calculation of a (continuous) map from a subinterval of $\mathbb{R}$ to itself. This result was illustrated in [14] on a three-link biped model (torso, two legs without knees). That model was sufficiently simple that it could be derived by hand and all of the hypotheses of the theory checked in an elementary manner. The robot under study here, on the other hand, is sufficiently complex that the equations of motion must be obtained symbolically.[4] The equations of motion fill several pages of dense type. Nevertheless, a controller with provable stability properties can still be designed. To illustrate some of the design flexibility available in this approach, a second controller is designed on the basis of optimal time-trajectories developed in [6], where limitations on torque and power have been addressed for the same robot. This controller, like the first one, is time-invariant and has provable stability properties.

The second objective of the paper is to investigate robustness of the closed-loop system by evaluating the performance of the robot in different situations. First, the behavior of the robot is studied when there is an obstacle on the ground and when there is an external force acting on its hips or torso. The goal is to demonstrate that the region of attraction of the periodic orbit is nonnegligible. Secondly, the robustness is checked by supposing that the robot is walking on a compliant surface. The formal stability analysis of the robot in closed-loop with the controller has been performed under the hypotheses that the contact between the leg end and the ground is rigid (perfectly inelastic) and the double support phase is instantaneous. The advantage of assuming a rigid contact model is that it considerably lowers the dimension of the model of the robot and the walking surface. In particular, there is a reduction in the number of DOF of the robot model (since the stance leg acts as a pivot, two DOF are removed), and the forces on the feet are determined by an algebraic equation instead of differential equations. This reduction in dimension greatly simplifies the feedback design and the stability analysis. Nevertheless, a realistic walking surface will be compliant and the ends of the legs may slip when in contact with ground. It is thus interesting to determine whether the design hypothesis of a rigid contact is valid. To check this, the controller designed on the basis of a rigid walking surface is applied to a model that includes compliance and dynamic friction of the walking surface. Through simulation, it is verified that if the walking surface is sufficiently stiff then the resulting walking motion is very similar to that obtained under the hypothesis of a rigid contact.

[4]The authors used the Symbolic Toolbox in MATLAB for this. The full model is available online at www.eecs.umich.edu/~grizzle/.

The remainder of the paper is structured as follows. Section II develops the dynamical model of the five-link robot and specifies all of the mechanical parameters; the model corresponds to a prototype that is under construction. The swing phase model is based on Lagrangian mechanics and has not yet been experimentally validated. As discussed above, a rigid model is used for the contact between the swing leg and ground and the double support phase is assumed to be instantaneous. The contact between the support leg and the ground is modeled as a pivot, and thus, during the single support phase, the model has five DOF. Section III develops the controller. The desired posture of the robot throughout a step is first parameterized in terms of a scalar function of the configuration variables of the robot, instead of time. From this, a set of outputs is constructed in such a way that the nulling of the outputs is equivalent to achieving the desired posture. The feedback design is completed by combining ideas from finite-time stabilization and computed torque to asymptotically null the outputs. The controller's performance is first evaluated by simulation in Section IV under the hypotheses of a rigid contact model, an instantaneous double support phase, and no slipping of the support leg. The simulations indicate that the controller induces an asymptotically stable walking motion of 0.6 m/s, but requires peak torques that are very near the maximal capability of the prototype. The actual stability of the induced walking motion is formally proven in Section V. A method to incorporate optimal time trajectories [6] into a time-invariant controller design is illustrated in Section VI, yielding a controller that meets natural design constraints. Section VII evaluates the controller's performance, first by supposing perturbations like a change in ground height or an external force acting on the hips, and second, by considering a compliant walking surface. For the latter case, the simulations are performed on a more detailed simulator developed by the French Project Commande de Robots à Pattes.[5] The main novelty of the detailed simulator is the inclusion of a nonlinear, compliant model of the contact between the robot's limbs and the ground [5], [20], [29] and a dynamic friction model [4], [28], [38]. The detailed simulator thus exercises all seven of the robot's DOF (the angles of the five links plus the Cartesian coordinates of the hips), and therefore serves as an independent check of the validity of the key hypotheses made in the mathematical derivation of the controller; in particular, the contact points of the limbs may slip and/or rebound, and the double support phase is not instantaneous. The controller's performance on the more complete model is shown to be similar to that obtained under the idealized hypotheses of Sections IV and V. Additional supporting plots and animations of the various controllers studied here can be found at http://www.eecs.umich.edu/~grizzle/.

II. Robot Model

The model is based on a prototype, named RABBIT; see[6] Fig. 1.

[5][Online.] Available: http://www-lag.ensieg.inpg.fr/recherche/cser/PRC-Bipedes/Prototype/rabbit.html

[6]The RABBIT prototype is used as testbed by the French Project Commande de Robots à Pattes of the CNRS-GdR Automatique.

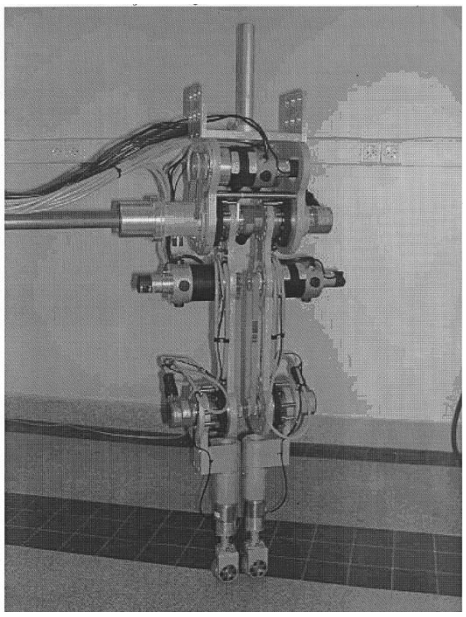

Fig. 1. Photo of RABBIT prototype.

The prototype has four independent actuators: the axis between the torso and each thigh is actuated as is the axis of each knee. The actuators have been sized so that the robot is capable of generating motions of at least 5 km/h when walking and 12 km/h when running. These speeds compare well with the capabilities of humans [7]. Many of the technical considerations that went into the design of the robot are summarized in [7]. The principal motivations for constructing the prototype were to study modeling (especially hybrid mechanical systems and compliant contact models), determination of optimal trajectories, limit cycles, stabilization of trajectories and the transition between walking and running.[7]

The prototype is limited to motion in the sagittal plane by means of a radial bar. The ends of the robot's legs are fitted with wheels turned normal to the sagittal plane so that radial movements of the contact points between the robot's legs and the floor are completely free; as the wheels are in the frontal plane, no mobility exists between the legs and the "feet" in the sagittal plane. The radius of the circular path imposed by the bar is approximately 3 m. The design of stabilizing controllers for the lateral motion of a walking robot has been addressed in [25], where it is shown that stability can be achieved by actively adjusting the lateral distance between the feet; this issue is not studied here.

The robot is modeled as a planar biped consisting of a torso, hips, and two identical legs with knees, but no ankles. It thus has seven DOF (the five joint angles plus the Cartesian coordinates of the hips, for example). It is supposed that the robot walks from left to right and that there is no rebound nor slip between the leg ends and the walking surface. Under this assumption, during the swing phase (only one leg touching the walking surface), the hip coordinates are not independent of the angular coordinates and thus the number of DOF decreases to five. A torque is applied between each leg and the torso, and a torque is applied at each knee. Thus, during the single support phase the robot is under actuated: there are 5-DOF and four actuators. It is supposed that all links and joints are rigid; in particular, there is no elasticity between the actuators and link joints [12], [26], [49]. It is assumed that the walking cycle takes place in the sagittal plane and consists of successive phases of single support.

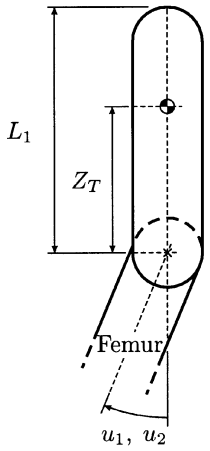

Fig. 2. Schematic of biped robot torso.

The complete model of the biped robot consists of two parts: the differential equations describing the dynamics of the robot during the swing phase (these equations are derived using the method of Lagrange [43]), and an impulse model of the contact event (the impact between the swing leg and the ground is modeled as a contact between two rigid bodies [21]). The contact between the stance leg and the ground is modeled as a pivot. As in [14] and [15], the complete model can be expressed as a nonlinear system with impulse effects [48].

A. Swing Phase Model

The dynamic model of the robot between successive impacts is derived from the Lagrange formalism[8]

$$D(q)\cdot\ddot{q}+C(q,\dot{q})\cdot\dot{q}+G(q)=B\cdot u \tag{1}$$

with $q = (q_{31}, q_{41}, q_{32}, q_{42}, q_1)'$ (see Fig. 4) and $u = (u_1, u_2, u_3, u_4)'$ (see Figs. 2 and 3). The torques u_1, u_2, u_3, and u_4 are applied between the torso and the stance leg, the torso and the swing leg, at the knee of the stance leg and at the knee of the swing leg, respectively. The model can be written in state space form by defining

$$\begin{aligned}\dot{x} &:= \begin{bmatrix} \omega \\ D^{-1}(q)\left(-C(q,\omega)\omega - G(q) + Bu\right)\end{bmatrix} \\ &=: f(x)+g(x)\cdot u\end{aligned} \tag{2}$$

where $\omega := \dot{q}$, and $x := (q', \omega')'$. The state space of the model will be restricted to physically reasonable values of q for

[7][Online.] Available: http://www-lag.ensieg.inpg/fr/recherche/cser/PRC-Bipedes/Prototype/rabbit.html

[8]The symbolic computation of the model is available at http://www.eecs.umich.edu/~grizzle/.

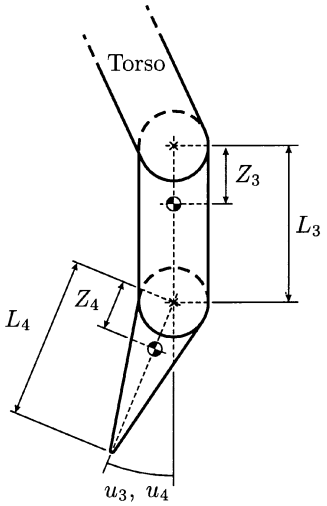

Fig. 3. Schematic of biped robot leg.

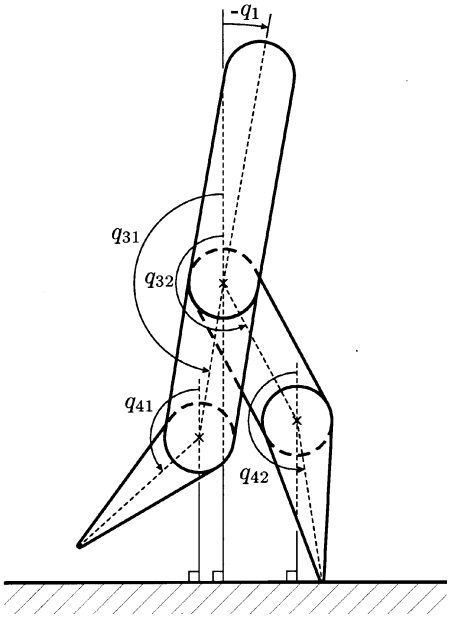

Fig. 4. Schematic of biped robot; absolute angles.

walking. To define these bounds, it is convenient to introduce the coordinates (p_{31}, p_{41}, p_{32}, p_{42}) (see Fig. 5) where

$$\begin{bmatrix} p_{31} \\ p_{41} \\ p_{32} \\ p_{42} \end{bmatrix} = \begin{bmatrix} \frac{1}{2}(q_{31}+q_{41}) \\ \pi + q_{41} - q_{31} \\ \frac{1}{2}(q_{32}+q_{42}) \\ \pi + q_{42} - q_{32} \end{bmatrix}. \tag{3}$$

Note that, for the computation of (3), it is assumed that the tibia and the femur are of equal length (as is the case of the prototype RABBIT). The variable p_{31} (resp. p_{32}) is the angle between the vertical axis and a "virtual" leg joining the hips to the foot of the stance leg (resp. the swing leg) and the variable p_{41} (resp. p_{42}) is the relative angle of the stance leg (resp. swing leg) knee. The state space for the system will be taken as $\mathcal{X} := \{(q',\omega')' | q \in M,\ \omega \in \mathbb{R}^5\}$, where $M = \{q | -\pi/2 < q_1 < \pi/2,\ (3\pi)/(4) < p_{31} < (5\pi)/(4),\ 0 < p_{41} < \pi,\ (3\pi)/(4) < p_{32} < (5\pi)/(4),\ 0 < p_{42} < \pi\}$. With this choice of M, the

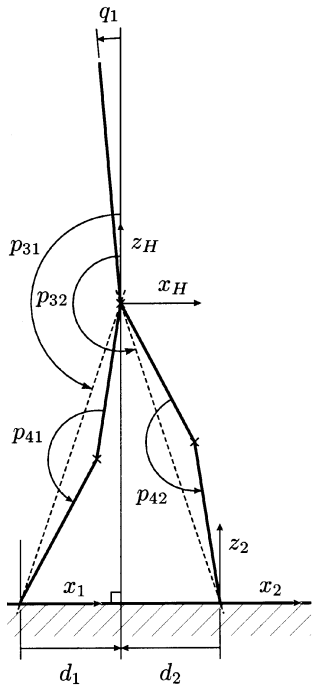

Fig. 5. Schematic of biped robot; relative angles.

robot's torso and support leg are never below the walking surface, which is taken as $\{(q,\omega) \in \mathcal{X} | z_1 = 0\}$, the set of points where the height of the end of the support leg is zero (for definition of z_1, see Fig. 5).

B. Impact Model

An impact occurs when the swing leg touches the walking surface, also called the ground. The impact between the swing leg and the ground is modeled as a contact between two rigid bodies. The development of the impact model requires the full seven DOF of the robot. Let us add Cartesian coordinates (x_H, z_H) to the hips (see Fig. 5). One then obtains the following extended model

$$D_e(q_e)\ddot{q}_e + C_e(q_e,\dot{q}_e)\dot{q}_e + G_e(q_e) = B_e u + \delta F_{ext} \tag{4}$$

with $q_e = (q_{31}, q_{41}, q_{32}, q_{42}, q_1, x_H, z_H)'$. δF_{ext} represents the external forces acting on the robot at the contact point. The basic hypotheses are: the contact of the swing leg with the ground results in no rebound and no slipping of the swing leg; at the moment of impact, the stance leg lifts from the ground without interaction; the impact is instantaneous; the external forces during the impact can be represented by impulses; the impulsive forces may result in an instantaneous change in the velocities, but there is no instantaneous change in the positions; and the torques supplied by the actuators are not impulsional.

From these hypotheses, the angular momentum is conserved about the impact point. One deduces

$$D_e(\dot{q}_e^+ - \dot{q}_e^-) = F_{ext} \tag{5}$$

where F_{ext} is the result of the contact impulse forces. $\dot{q}_e^+$ (resp. $\dot{q}_e^-$) is the velocity just after (resp. before) impact. An additional set of two equations is obtained by supposing that the stance leg does not rebound nor slip at impact. Then, from the condition

that the swing leg does not rebound nor slip at impact, one obtains

$$\frac{d}{dt}E(q_e) = \frac{\partial E}{\partial q_e} \cdot \dot{q}_e^+ = 0. \tag{6}$$

$E(q_e) = (x_2, z_2)'$ the Cartesian coordinates of the end of the swing leg. The result of solving (5) and (6) yields an expression for $\dot{q}_e^+$ in term of $\dot{q}_e^-$.[9] The final result is an expression for $x^+ := (q^+, \omega^+)$ (state value just after the impact) in terms of $x^- := (q^-, \omega^-)$ (state value just before the impact), which is expressed as

$$x^+ = \Delta(x^-). \tag{7}$$

C. Nonlinear System With Impulse Effects

The overall biped robot model can be expressed as a nonlinear system with impulse effects [48]

$$\begin{aligned} \dot{x} &= f(x) + g(x) \cdot u \quad x^- \notin S \\ x^+ &= \Delta(x^-) \quad x^- \in S \end{aligned} \tag{8}$$

where

$$S := \{(q, \omega) \in \mathcal{X} | z_2 = 0, x_2 > 0\}. \tag{9}$$

The condition $z_2 = 0$ defines a contact event between the swing leg end and the ground, while $x_2 > 0$ imposes that the swing leg touches in front of the stance leg. Solutions of (8) are taken to be right continuous (see [14] for details). With this convention, as long as the robot is initialized in $\mathcal{X}$ with the swing leg on or above the walking surface, all valid solutions of the model result in the robot remaining on or above the walking surface.

III. Feedback Controller Design

This section develops the extension of the controller of [14], [15] for the five-link biped with knees. The fundamental idea is to encode walking in terms of a set of "posture conditions", which are in turn expressed as "holonomic constraints" on the position variables. These "constraints" are then used to construct outputs of the mechanical model and are "imposed" on the robot via feedback control. The controller is designed on the basis of the assumptions made in Section II, namely that the impact model is rigid and the double support phase is instantaneous. These hypotheses will be revisited in Section VII.

A. Output Definition

In human walking, one observes that the torso is maintained at a nearly vertical angle, the hips remain roughly centered between the feet and at a nearly constant height above the walking surface, and the end of the swing leg traces an approximately parabolic trajectory. In addition, the knees are never hyperextended (as opposed to a bird) and only slightly flexed (as opposed to a monkey). These observations have been used to build a set of control objectives through the following output functions which will be driven to zero (or to numerically small values):

$$y = h(q) := \begin{bmatrix} h_1 \\ h_2 \\ h_3 \\ h_4 \end{bmatrix} = \begin{bmatrix} k_1 \cdot (q_1 - q_{1d}) \\ k_2 \cdot (d_1 + d_2) \\ k_3 \cdot (z_H - z_{Hd}(d_1)) \\ k_4 \cdot (z_2 - z_{2d}(d_1)) \end{bmatrix}. \tag{10}$$

In the above, the Cartesian coordinates of the hips, (x_H, z_H), and the end of the swing leg, (x_2, z_2), are expressed in the coordinate frame of the foot of the stance leg, (x_1, z_1) (see Fig. 4)

$$\begin{aligned} x_1 &= 0 \\ z_1 &= 0 \\ x_H &= L_3 \cdot \sin(q_{31}) + L_4 \cdot \sin(q_{41}) \\ z_H &= -L_3 \cdot \cos(q_{31}) - L_4 \cdot \cos(q_{41}) \\ x_2 &= x_H - L_3 \cdot \sin(q_{32}) - L_4 \cdot \sin(q_{42}) \\ z_2 &= z_H + L_3 \cdot \cos(q_{32}) + L_4 \cdot \cos(q_{42}) \\ d_1 &= x_H - x_1 = L_3 \cdot \sin(q_{31}) + L_4 \cdot \sin(q_{41}) \\ d_2 &= x_H - x_2 = L_3 \cdot \sin(q_{32}) + L_4 \cdot \sin(q_{42}). \end{aligned} \tag{11}$$

The output y_1 is chosen to maintain the angle of the torso at a desired constant value, say q_{1d}. The output y_2 ensures the advancement of the hips while the swing leg goes from behind the stance leg to in front of it (see Fig. 5 for the definition of d_1 and d_2). The output y_3 controls the hip height in such a way that the hips can rise and fall by a small amount in a natural way. The desired trajectory z_{Hd} of the hips is defined as a second order polynomial of d_1 such that $d_1 \in [-\mathrm{sld}/2, \mathrm{sld}/2]$, where sld is the desired step length, $z_{H\mathrm{MAX}}$ (resp. $z_{H\mathrm{MIN}}$) is the maximum (resp. minimum) desired value of z_H over a step and $z_{Hd}(-\mathrm{sld}/2) = z_{H\mathrm{MIN}}$, $z_{Hd}(0) = z_{H\mathrm{MAX}}$, $z_{Hd}(\mathrm{sld}/2) = z_{H\mathrm{MIN}}$. The hip trajectory has not been chosen by optimization, though it seems quite natural that the hips are highest at mid-gait and lowest at foot touchdown and liftoff. The output y_4 controls the trajectory of the end of the swing leg; the desired trajectory z_{2d} is defined as a second order polynomial of d_1 such that $d_1 \in [-\mathrm{sld}/2, \mathrm{sld}/2]$, where $z_{2\mathrm{MAX}}$ is the maximum desired value of z_2 over a step and $z_{2d}(-\mathrm{sld}/2) = 0$, $z_{2d}(0) = z_{2\mathrm{MAX}}$, $z_{2d}(\mathrm{sld}/2) = 0$. The foot trajectory also has not been chosen by optimization, but seems to correspond to natural walking gait. The gains k_1, k_2, k_3, and k_4 are constant values to be chosen later.

B. Controller Synthesis

The control objective is to drive the outputs (10) to zero. Since the outputs (10) only depend on the generalized positions, q, and the dynamic model (2) is second order, the relative degree of each output component is at least two. Using standard Lie derivative notation [22], [43], direct calculation yields

$$\ddot{y} = L_f^2 h(x) + L_g L_f h(x) \cdot u. \tag{12}$$

For the moment, it is supposed that the matrix $L_g L_f h$ is invertible on the region of interest. This will be confirmed later in the paper. The method of computed torque (or inverse dynamics) can then be used to define $v := L_f^2 h + L_g L_f h \cdot u$, resulting in

[9] The solvability of the equations is easily verified; see [14].

four double integrators $\ddot{y}_i = v_i$, $i = 1$ to 4. One possible approach to control design would be to design asymptotically stabilizing controllers, such as $v_i = k_{i1}y_i + k_{i2}\dot{y}_i$, for the double integrators. In general, when such a feedback is applied to the full hybrid model (8), it is no longer able to drive the outputs (10) asymptotically to zero due to the impulsive effects of the impacts. A general means of trying to "overcome" this can be observed in the literature: for experimental as well as simulation based studies, the feedback gains appear to be universally chosen sufficiently large so that the time constant for driving the controlled quantities to their reference values is much less than the time interval of a step. A biological basis for doing this is much more difficult to establish because the experiments are not easy to do well. Nevertheless, the evidence suggests that if a perturbation is deliberately introduced in a human's gait [8], [9], the subject's gait will recover in just a few cycles, suggesting high-gain control.

The use of high-gain control can be made to work quite well in simulation. The difficulty comes in mathematically analyzing the existence and stability of periodic orbits induced by the controller. Since we are dealing with periodic orbits, Poincaré's method is the appropriate tool. However, to apply it one must compute the induced discrete-time dynamics from a hyper-surface transversal to the orbit back to the hyper-surface [16], [32]. The induced discrete-time dynamics is called the Poincaré map. In the case of the model (8), the hyper-surface has dimension nine and the computation of the Poincaré map is impractical. The key idea established in [14] is that for a mechanical system with N-DOF and m-independent inputs, the feedback control design can be carried out in a way that greatly simplifies the stability analysis problem: the dimension of the image of the Poincaré map can be reduced from $2N-1$ to $2(N-m)-1$. For the biped considered here, this results in a one-dimensional analysis problem. The Poincaré map for this one-dimensional problem must still be computed numerically. The main points are that its numerical computation is very easy and it leads to conclusive existence and stability properties for periodic orbits.

The feedback design proceeds as follows. Define a continuous[10] feedback $v = v(y, \dot{y})$ on (12) so that each of the four double integrators $\ddot{y}_i = v_i$ is (globally) finite-time stabilized. The feedback functions used here come from [2]

$$v = \Psi(y, \dot{y}) := \frac{1}{\epsilon} \cdot \begin{bmatrix} \psi_1(y_1, \epsilon \cdot \dot{y}_1) \\ \psi_2(y_2, \epsilon \cdot \dot{y}_2) \\ \psi_3(y_3, \epsilon \cdot \dot{y}_3) \\ \psi_4(y_4, \epsilon \cdot \dot{y}_4) \end{bmatrix}. \tag{13}$$

[10]The theory in [14], [15] does NOT allow the use a discontinuous feedback as is commonly used in sliding mode control.

Each function $\psi_i(y_i, \epsilon \cdot \dot{y}_i)$, $i = 1$ to 4, is defined as

$$\begin{aligned} \psi_i := & -\operatorname{sign}\left(\phi_i(y_i, \epsilon \cdot \dot{y}_i)\right) \cdot \left|\phi_i(y_i, \epsilon \cdot \dot{y}_i)\right|^{\frac{\alpha}{2-\alpha}} \\ & -\operatorname{sign}(\epsilon \cdot \dot{y}_i) \cdot |\epsilon \cdot \dot{y}_i|^{\alpha} \end{aligned} \tag{14}$$

with $\phi_i(\cdot) = y_i + (1/2 - \alpha)\operatorname{sign}(\epsilon \cdot \dot{y}_i) \cdot |\epsilon \cdot \dot{y}_i|^{2-\alpha}$ and $0 < \alpha < 1$. The real parameter $\epsilon > 0$ allows the settling time of the controllers to be adjusted. The overall feedback applied to (8) is given by

$$u := (L_g L_f h)^{-1} \left(\Psi(h, L_f h) - L_f^2 h\right). \tag{15}$$

This is the method of computed torque with a finite-time stabilizing controller on each of the double integrators.

IV. Simulations

Consider the biped robot model (8) with the following parameter values[11] (see Figs. 2 and 3); suppose in addition that the actuators at the knees and at the hips have a gear ratio of 50:1, with a rotor inertia of 0.83 kg.m^2. The mechanical parameters can be found online at http://www-lag.ensieg.inpg/fr/recherche/cser/PRC-Bipedes/Prototype/rabbit.html. Consider the feedback of Section III-B with the parameters shown in the table at the bottom of the page. The robot was initialized in double support with an initial hip velocity, v_H^- (i.e., the velocity just before impact), of 0.90 m/s. This choice is justified[12] in Section V: in fact, the closed-loop system stability analysis shows that the system is stable if v_H^- is taken between 0.85 m/s and 1.25 m/s (see Section V and Fig. 13), and also that v_H^- is close to 1.02 m/s on the limit cycle. Note also that the average velocity of the biped equals about 0.6 m/s on the limit cycle. In the feedback (15), $\epsilon = 0.06$ and $\alpha = 0.9$. The parameter $\epsilon > 0$ allows the settling time of the controller to be adjusted and $0 < \alpha < 1$ achieves a finite-settling time.

Several aspects of the solution corresponding to the model and feedback with the above parameters are now highlighted. Simulations were performed in the MATLAB/Simulink environment, using the ode45 integration algorithm with variable step size. Fig. 6 displays the outputs and shows that the controller drives them to zero before impact. This implies that the posture constraint encoded in the output function (10) is satisfied and that the proof of stability to be presented in the next

[11][Online.] Available: http://www-lag.ensieg.inpg/fr/recherche/cser/PRC-Bipedes/Prototype/rabbit.html

[12]Extensive simulations are not performed here to verify stability because an analytical proof is provided in the next section. However, supporting plots and animations are available at http://www.eecs.umich.edu/~grizzle/.

Output	Gain	Parameters
y_1	$k_1 = 62.5$	$q_{1d} = -\pi/30\text{rad}$
y_2	$k_2 = 500$	
y_3	$k_3 = 1$	$z_{H\text{MIN}} = 0.76\,m,\ z_{H\text{MAX}} = 0.79\,m,$
y_4	$k_4 = 1$	$z_{2\text{MAX}} = 20\,mm,\ \text{sld} = 0.45\,m$

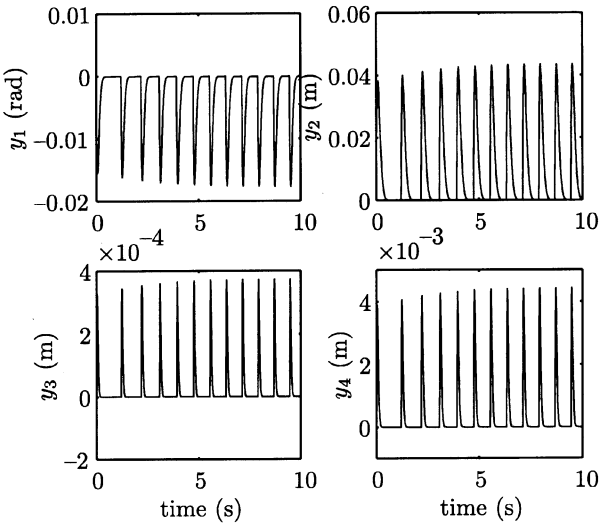

Fig. 6. Plot of outputs versus time. Each output is driven to zero within a single stride.

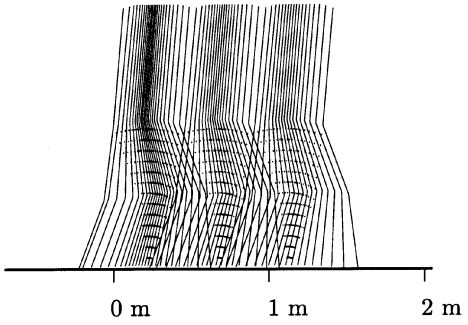

Fig. 7. Plot of walking as a sequence of stick figures.

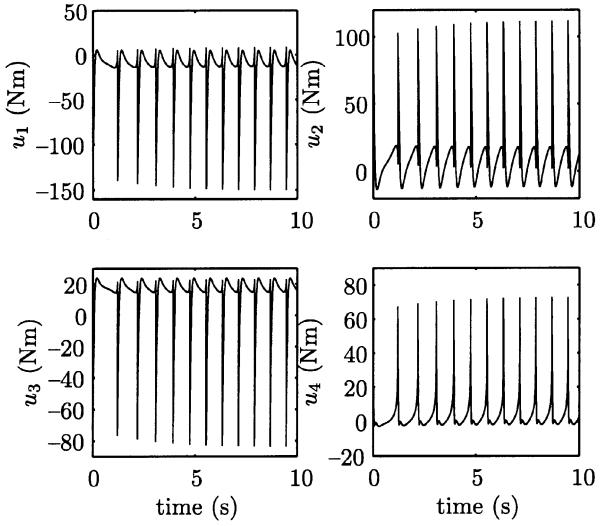

Fig. 8. Plot of applied torques (in Newton meters) versus time.

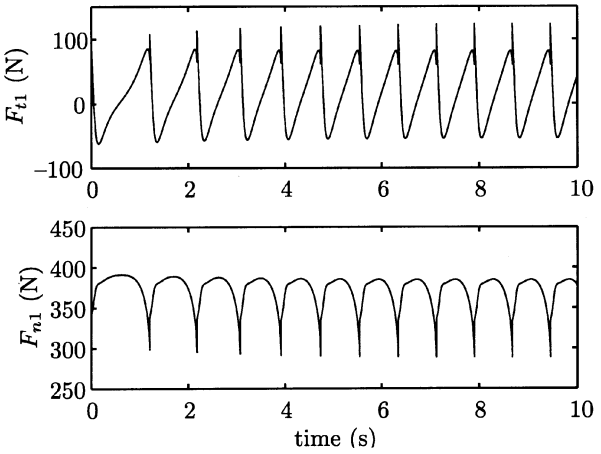

Fig. 9. Plot of normal (bottom) and tangential (top) forces (in Newtons) acting on the stance leg end versus time.

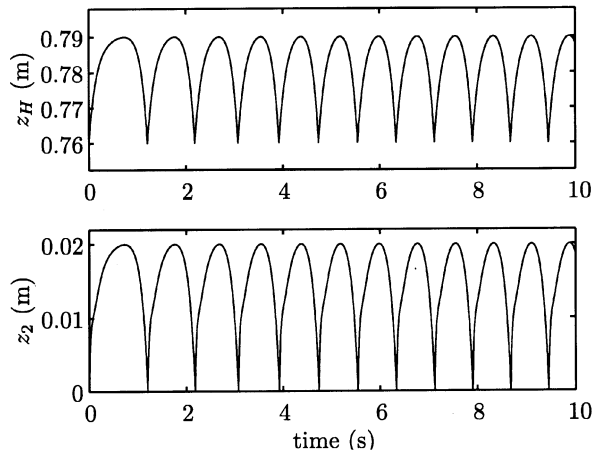

Fig. 10. Plot of z_H and z_2 (in meters).

section can be applied. Fig. 7 displays the walking motion of the biped robot as a series of stick figures over three steps. The walking appears to be natural, i.e., how a human without arms might walk. Fig. 8 displays the applied torques over a few walking cycles; note that the peak torque magnitude is around 150 Nm on the limit cycle. Fig. 9 displays the normal and tangential forces acting on the stance leg end; note that the maximum force is less than 400 N. Fig. 10 displays the coordinates z_2 (vertical height of the end of the swing leg) and z_H (vertical height of the hips), which are key quantities in the definition of the outputs used to generate the feedback controller. From the plot of z_H it is observed that the gait is "compass-like" in that the hips are highest at mid stance and lowest at foot touchdown/liftoff.

From Figs. 6–10, the walking trajectories appear to be asymptotically stable: after several steps, the robot seems to reach a limit cycle. This appearance will proved in the following section. In the sequel, robustness of the feedback is investigated versus ground height variations and external perturbations; that is, the robot still walks with moderate perturbations (see Section VII). The output function chosen, (10), is certainly not unique; for example, appropriately controlling torso angle, horizontal hip placement, and swing and stance leg knee angles will also yield a stable walking motion. In order to use the controller on RABBIT, it is interesting (for achieving greater autonomy of the robot) to decrease the energy used for walking. This will be addressed in Section VI.

V. Stability Proof

The purpose of this section is to prove the asymptotic stability or instability of trajectories resulting from the biped in closed loop with the controller (15). An important result from [14] is that stability (or instability) can be proven on the basis of the restriction of the Poincaré map to a one-dimensional manifold. In the following, only the bare minimum of mathematical notation needed to use this tool will be introduced. The reader seeking a careful development of these ideas is referred to [14]. The steps followed here would be the same for any N-link biped with $N-1$ independent actuators.

Let Z denote the zero dynamics manifold, i.e., $Z = \{(q,\dot{q}) \in \mathcal{X} | h(q) = 0,\ L_f h(q) = 0\}$, and recall that $S := \{(q,\omega) \in \mathcal{X} | z_2 = 0,\ x_2 > 0\}$. The conditions required to define the restricted Poincaré map are:

1) $S \cap Z$ is a smooth submanifold of $\mathcal{X}$;
2) the decoupling matrix $L_g L_f h$ is invertible;
3) the convergence time of the controller is strictly less than the time of a single step of the robot.

A. Smoothness of $S \cap Z$

From standard results in [3], $S \cap Z$ will be a smooth one-dimensional manifold if the map

$$\begin{bmatrix} h(q) \\ L_f h(q,\dot{q}) \\ z_2(q) \end{bmatrix} \tag{16}$$

has constant rank[13] equal to nine on $S \cap Z$. A simple argument shows that this is equivalent to the rank of $[h(q)' \quad z_2(q)]'$ being equal to five. Hence, define the 5×5 matrix $A = [(\partial h/\partial q) \ (\partial z_2/\partial q)]$ whose determinant in the p coordinates is proportional to $[\sin(p_{42})\sin(p_{31})\sin(p_{41}/2)\sin(p_{41})]$. On M, it is easily verified that the determinant vanishes only at $p_{31} = \pi$. However, if $q \in Z$ and $p_{31} = \pi$, then $z_2(q) = 0.01 \neq 0$, and thus $q \notin S$. Hence, the determinant of A is nonzero on $S \cap Z$. If $(q,\omega) \in S \cap Z$, then it follows that q is equal to a constant; call this value q_0. Furthermore, it follows that ω is parameterized by a single variable. This parameterization is developed next. Let $\Phi(q) = [h(q) \ x_H(q)]$, where x_H is the horizontal position of the robot's hips. It is straightforward to verify that Φ has full rank at q_0. On Z, it follows that $(d/dt)h(q) = L_f h(q,\omega) = 0$, and thus

$$\begin{bmatrix} 0 \\ v_H \end{bmatrix} = \frac{d}{dt}\Phi(q) = \frac{\partial \Phi}{\partial q} \cdot \omega. \tag{17}$$

Thus, $\sigma : \mathbb{R} \to S \cap Z$ by

$$\sigma(v_H^-) := \begin{bmatrix} q_0 \\ \left[\frac{\partial \Phi(q_0)}{\partial q}\right]^{-1} \cdot v_H^- \end{bmatrix} \tag{18}$$

is a diffeomorphism from $\mathbb{R}$ to $S \cap Z$, with v_H^- the horizontal velocity of the hips just before impact.

[13]Recall that the rank of a map at a point is by definition the rank of its Jacobian matrix evaluated at the same point.

B. Proving Invertibility of the Decoupling Matrix

The complexity of the decoupling matrix, $L_g L_f h$, makes a direct proof of invertibility highly nontrivial. Moreover, since the point $q_{ext} = (\pi,\pi,\pi,\pi,0)'$ is an extremum of the height of the hips, the decoupling matrix for the choice of outputs (10) is necessarily singular at $q_{\rm ext}$. Hence, a proof of the invertibility of the decoupling matrix must be local in q. One method of local proof is to demonstrate sign definiteness of the decoupling matrix's determinant in an open set about the biped's trajectories. Sign definiteness implies the determinant never equals zero in that set and, hence, in that set, the decoupling matrix is invertible. This is the method used here. The proof is carried out in two steps. In the first step, the decoupling matrix is simplified by the application of an invertible feedback [37] to the model.[14] In the second step, elementary bounds on the individual terms appearing in the determinant of the decoupling matrix are determined and used to compute upper and lower bounds on the determinant of the decoupling matrix. To apply the technique of [37], it is easiest to work in relative coordinates $\bar{q} := (\bar{q}_{31}, \bar{q}_{41}, \bar{q}_{32}, \bar{q}_{42}, q_1)'$ where

$$\begin{bmatrix} \bar{q}_{31} \\ \bar{q}_{41} \\ \bar{q}_{32} \\ \bar{q}_{42} \end{bmatrix} = \begin{bmatrix} q_{31} - q_1 \\ q_{31} - q_{41} \\ q_{32} - q_1 \\ q_{32} - q_{42} \end{bmatrix}. \tag{19}$$

Denote the dynamic model (1) in these new coordinates as

$$\bar{D}(\bar{q}) \cdot \ddot{\bar{q}} + \bar{C}(\bar{q},\dot{\bar{q}}) \cdot \dot{\bar{q}} + \bar{G}(\bar{q}) = \bar{B} \cdot u. \tag{20}$$

It is easily shown that $\bar{B}$ has the form $\bar{B} = [I \ 0]'$. Next, partition the coordinates into $q_a = (\bar{q}_{31}, \bar{q}_{41}, \bar{q}_{32}, \bar{q}_{42})'$ and $q_b = q_1$, the "actuated" coordinates and "unactuated" coordinates, respectively. Write (20) as

$$\bar{D}_{11}(\bar{q})\ddot{q}_a + \bar{D}_{12}(\bar{q})\ddot{q}_b + \bar{C}_1(\bar{q},\dot{\bar{q}})\dot{q}_a + \bar{G}_1(\bar{q}) = u \tag{21}$$
$$\bar{D}_{21}(\bar{q})\ddot{q}_a + \bar{D}_{22}(\bar{q})\ddot{q}_b + \bar{C}_2(\bar{q},\dot{\bar{q}})\dot{q}_a + \bar{G}_2(\bar{q}) = 0 \tag{22}$$

and solve (22) for $\ddot{q}_b$ as

$$\ddot{q}_b = -\bar{D}_{22}(\bar{q})^{-1}\left(\bar{D}_{21}(\bar{q})\ddot{q}_a + \bar{C}_2(\bar{q},\dot{\bar{q}})\dot{q}_a + \bar{G}_2(\bar{q})\right). \tag{23}$$

Substituting (23) into (21) yields

$$\hat{D}(\bar{q})\ddot{q}_a + \hat{C}(\bar{q},\dot{\bar{q}})\dot{q}_a + \hat{G}(\bar{q}) = u \tag{24}$$

where[15]

$$\hat{D}(\bar{q}) = \bar{D}_{11}(\bar{q}) - \bar{D}_{12}(\bar{q})\bar{D}_{22}^{-1}(\bar{q})\bar{D}_{21}(\bar{q}) \tag{25}$$
$$\hat{C}(\bar{q},\dot{\bar{q}}) = \bar{C}_1(\bar{q},\dot{\bar{q}}) - \bar{D}_{12}(\bar{q})\bar{D}_{22}^{-1}(\bar{q})\bar{C}_2(\bar{q},\dot{\bar{q}}) \tag{26}$$
$$\hat{G}(\bar{q}) = \bar{G}_1(\bar{q}) - \bar{D}_{12}(\bar{q})\bar{D}_{22}^{-1}(\bar{q})\bar{G}_2(\bar{q}). \tag{27}$$

Applying the partial linearizing feedback $u = \hat{D}(\bar{q})v + \hat{C}(\bar{q},\dot{\bar{q}})\dot{q}_a + \hat{G}(\bar{q})$ to (21) allows (21) and (22) to be rewritten as

$$\ddot{q}_a = v$$
$$\ddot{q}_b = -\bar{D}_{22}(\bar{q})^{-1}\left(\bar{D}_{21}(\bar{q})\ddot{q}_a + \bar{C}_2(\bar{q},\dot{\bar{q}})\dot{q}_a + \bar{G}_2(\bar{q})\right).$$

[14]By standard results in [22], the invertibility of the decoupling matrix is invariant under the application of invertible feedbacks.

[15]The invertibility of $\bar{D}_{22}$ is assured by the positive definiteness of D.

The previous model is feedback equivalent to the original system. It can be expressed in state space form with the same choice of x as before to obtain

$$\dot{x} = \hat{f}(x) + \hat{g}(x)v. \tag{28}$$

Since the rank of the decoupling matrix is invariant under invertible feedback, the decoupling matrices for systems (2) and (28) have the same rank. The determinant of the decoupling matrix for (28) can be directly computed and shown to be of the form[16]

$$\det L_{\hat{g}} L_{\hat{f}} h(\bar{q}) = \frac{\mathrm{N}um(\bar{q})}{\mathrm{D}en(\bar{q})} \tag{29}$$

with $\mathrm{N}um(\bar{q}) = \sum_{i=1}^{94} k_i^N g_i^N(c_i^N \bar{q})$ and $\mathrm{D}en(\bar{q}) = \sum_{i=1}^{9} k_i^D g_i^D(c_i^D \bar{q})$, where the k_i's are constants, g_i's are sine and cosine functions, and c_i's are row vectors in $\mathbb{R}^5$. For a given subset $\mathcal{O} \subset M$ (recall that M is the allowed set for the configuration variables), upper and lower bounds on the determinant of the decoupling matrix can be found via calculation of the minimum and maximum of each of the 103 terms of the numerator and denominator over $\mathcal{O}$. For example, if the denominator in (29) is positive, then

$$\begin{aligned} \max_{\bar{q}\in\mathcal{O}} \det L_{\hat{g}} L_{\hat{f}} h(\bar{q}) &\le \frac{\max_{\bar{q}\in\mathcal{O}} \mathrm{N}um(\bar{q})}{\min_{\bar{q}\in\mathcal{O}} \mathrm{D}en(\bar{q})} \\ &\le \frac{\max_{i\in I} \max_{\bar{q}\in\mathcal{O}_i} \mathrm{N}um(\bar{q})}{\min_{i\in I} \min_{\bar{q}\in\mathcal{O}_i} \mathrm{D}en(\bar{q})} \end{aligned} \tag{30}$$

where $\mathcal{O} \subset \bigcup_{i\in I} \mathcal{O}_i$, and the $\mathcal{O}_i$ are closed and bounded. The max and min operations in (30) are especially trivial to evaluate if the sets $\mathcal{O}_i$ are selected to be of the form

$$\mathcal{O}_i := \left\{ x | \bar{q}_{kl,i}^{\min} \le \bar{q}_{kl} \le \bar{q}_{kl,i}^{\max}, q_{1,i}^{\min} \le q_1 \le q_{1,i}^{\max} \right\}.$$

with $3 \le k \le 4$ and $1 \le l \le 2$. The above technique was applied to the apparent limit cycle of Section IV. Individual closed sets $\mathcal{O}_i$ were determined by dividing the time trajectory into disjoint pieces, and over bounding the configuration variables so that over the ith time interval, the trajectory of the configuration variables lies strictly in the interior of $\mathcal{O}_i$. As an illustration, Fig. 11 shows the result of this process for $\bar{q}_{31}$. Division of the trajectories in time into pieces over which the determinant could be proven to be sign definite was accomplished with a simple binary search algorithm. The results of this process gives the upper and lower bounds of the determinant of the decoupling matrix as well as the minimum and maximum of the determinant over each subset, and the beginning and end of each set's division in time. An example of this can be found online at http://www.eecs.umich.edu/~grizzle/. It should be noted that: 1) this process could be iterated to prove the decoupling matrix's invertibility over a larger subset of the biped's state space; and 2) the fact that this method works is not an accident. Standard compactness and continuity arguments can be used to show that the decoupling matrix is invertible on an open set about the configuration variable trajectories if and only if a there exists a set $\mathcal{O}$ which is the interior of a union of a finite number of closed sets $\mathcal{O}_i$ as described above.

[16]It is straightforward to check that the decoupling matrix depends only upon the configuration variables, q, and not on the angular velocities.

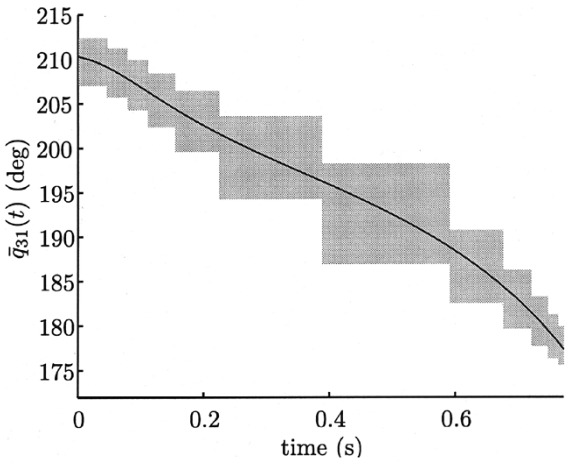

Fig. 11. Projection of the determined subsets $\mathcal{O}_i$ onto the $\bar{q}_{31}$ trajectory. Note that $\bar{q}_{31}(t)$ lies strictly within the union of the interiors of the subsets. The same is true of each of the other configuration variables.

C. The Restricted Poincaré Map

The cross section for the Poincaré map will be taken to be S, the impact surface. Let $P : S \to S$ be the usual Poincaré[17] map. For those trajectories for which the convergence time of the controller (15) is less than the time to make a single step, the trajectory will have converged to the zero dynamics manifold, Z, in finite time. In this case, P takes values in $S \cap Z$. The restricted Poincaré map is defined to be $\rho : S \cap Z \to S \cap Z$ by $\rho(x) = P(x)$; that is $\rho := P|_{S\cap Z}$. To compute ρ, it is easiest to use the identification of $S \cap Z$ with $\mathbb{R}$ given by (18). Thus, define $\lambda : \mathbb{R} \to \mathbb{R}$ by $\lambda := \sigma^{-1} \circ \rho \circ \sigma$. The function λ can be computed in a straightforward manner.

Restricted Poincaré map: $\lambda : \mathbb{R} \to \mathbb{R}$

1) Let $v_H^- > 0$ denote the horizontal velocity of the robot's hips just before impact (the restriction to positive velocities corresponds to the robot walking from left to right). Compute $x^- := \sigma(v_H^-) \in S \cap Z$, the position of the robot just before impact.
2) Apply the impact model to x^-, that is, compute $x^+ := \Delta(x^-)$.
3) Use x^+ as the initial condition in (2) controlled by (15), the robot in closed loop with the controller, and simulate until one of the following happens:
   a) There exists a (first) time $T > 0$ where $z_2(T) = 0$. If T is greater than the settling time of the controller, then $\lambda(v_H^-) := v_H^+(T)$; else, $\lambda(v_H^-)$ is undefined at this point.
   b) There does not exist a $T > 0$ such that $z_2(T) = 0$; in this case, it is also true that $\lambda(v_H^-)$ is undefined at this point. ■

D. Stability Results

To determine if the closed-loop system is stable under the controller (15), the function λ is computed for $v_H^- \in [0.5, 1.5]$. Fig. 12 displays the limit cycle over several steps with the pre-

[17]Since not every initial condition in S will result in the robot making a successful step, P is in general only a partial map; that is, its domain of definition is not all of S. The same is true, of course, for the restricted Poincaré map.

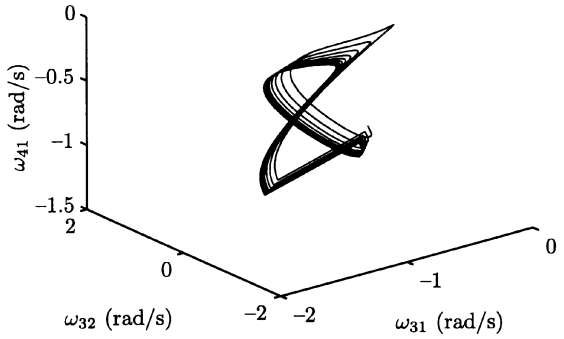

Fig. 12. Three-dimensional projection of the attractive orbit. The straight-line segment of the trajectory (near bottom) reflects the instantaneous change in velocity at the impact. The initial conditions are in the bottom right, outside the cycle.

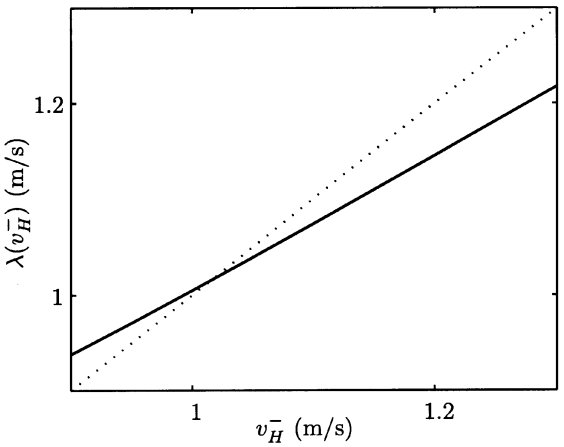

Fig. 13. Function λ (bold line) and identity function (dotted line) versus v_H^-. This graph establishes the existence of an asymptotically stable walking motion.

vious parameters of simulation, and with the initial hip velocity set to $v_H^- = 0.9$ m/s. The resulting trajectory converges to a limit cycle, supporting the stability analysis. Fig. 13 displays the function λ. One deduces that λ is undefined for v_H^- less than 0.85 m/s (because the robot does not have enough kinetic energy to make a step) and more than 1.25 m/s (because the robot is moving too fast for the outputs to converge in a single stride). A fixed point appears at approximately 1.02 m/s, and corresponds to an asymptotically stable walking cycle.

VI. Incorporating Known Optimal Trajectories Into the Control Law

There is a great deal of flexibility in how one chooses the outputs that are to be driven to zero. Furthermore, the choice of the (trajectories of the) outputs has a strong influence on the energy consumed by the system. In [6], optimal walking and running time-trajectories are analyzed for the same biped model, RABBIT. Following [14, Sect. V-A], these time trajectories can often be converted into output functions. Observe that in a normal walking motion, the angle p_{31} (see Fig. 5) will be strictly monotonically increasing (the horizontal position of the hips and often the angle of the tibia of the stance leg are also strictly monotonically increasing over a step). Once a strictly increasing generalized coordinate has been identified, it

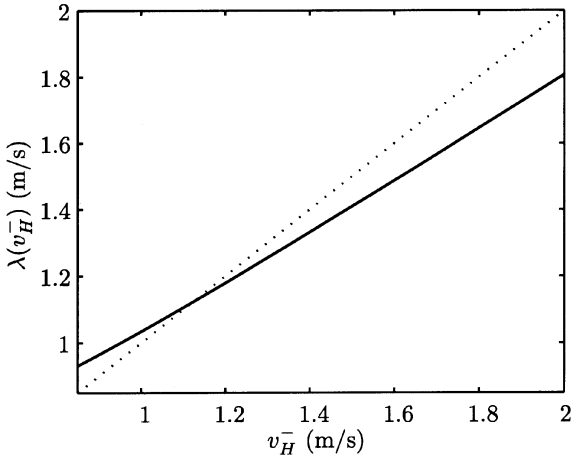

Fig. 14. Optimal trajectories. Function λ (bold line) and identity function (dotted line) versus v_H^-.

is always possible to re-parameterize the trajectories for the remaining generalized coordinates in terms of it. This procedure was carried out here for a walking motion of 0.75 m/s that is optimal with respect to consumed energy [6, Sect. 3.4], criteria C_3, where, in the optimization procedure, the actuator limitations and other constraints associated with the prototype have been taken into account.

As in Section III, the quantities to be controlled were taken as q_1, $d_1 + d_2$, z_H, and z_2. New outputs were posed in the form

$$\begin{aligned} y_1 &= q_1 - P_1(p_{31}) \quad y_2 = d_1 + d_2 - P_2(p_{31}) \\ y_3 &= z_H - P_3(p_{31}) \quad y_4 = z_2 - P_4(p_{31}) \end{aligned} \tag{31}$$

where each polynomial P_i is defined as

$$\begin{aligned} P_i = a_{0i} + a_{1i} \cdot p_{31} + a_{2i} \cdot p_{31}^2 + a_{3i} \cdot p_{31}^3 \\ + a_{4i} \cdot p_{31}^4 + a_{5i} \cdot p_{31}^5 + a_{6i} \cdot p_{31}^6. \end{aligned} \tag{32}$$

Coefficients a_{ij} are obtained by regressing these polynomials against the optimal time trajectories from [6].

Consider next the biped robot model (8) with the parameter values of Section IV, the above outputs, and the feedback of Section III. The initial velocity of the hips, v_H^-, is chosen as 1.6 m/s, in order to show that there is convergence to a limit cycle after several steps. This choice is justified by the stability analysis. Indeed, proceeding exactly as in Section V, it can be shown that:

- $S \cap Z$ is a smooth one-dimensional manifold;
- the decoupling matrix $L_g L_f h$ is invertible;
- the function $\lambda(v_H^-)$ has a fixed point and is defined over a reasonable domain (see Fig. 14).

The closed-loop system stability analysis based on $\lambda(v_H^-)$ shows that the system is stable if v_H^- is taken greater than 0.85 m/s, and that there is a limit cycle corresponding to v_H^- of about 1.1 m/s. The initial condition of $v_H^- = 1.6$ m/s does not start the system on the limit cycle, but the simulations show that the biped's motion converges to a limit cycle, corresponding to an average velocity of the biped equal to 0.75 m/s, and to hips velocity before the impact, v_H^-, equal to 1.1 m/s. Simulations therefore confirm the results derived from analysis of λ. The feedback (15) has been tuned with $\epsilon = 0.1$ and $\alpha = 0.9$.

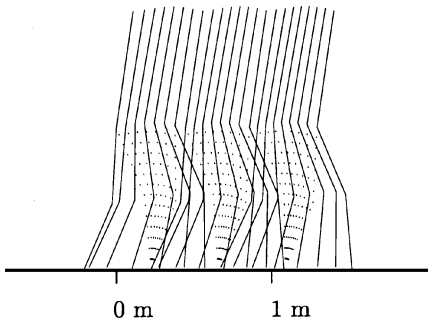

Fig. 15. Optimal trajectories. Plot of walking as a sequence of stick figures.

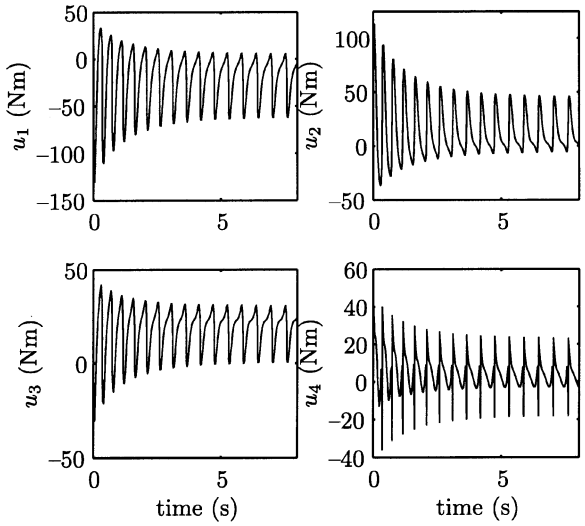

Fig. 16. Optimal trajectories. Plot of applied torques (in Newton meters) versus time.

The simulation verified that the controller successfully drives the outputs to zero before impact. Fig. 15 displays the walking motion of the biped robot as a series of stick figures over three steps. Fig. 16 displays the applied torques over a few steps; note that the peak torque magnitude on the limit cycle is now about 60 Nm, which is compatible with the prototype's torque limits, and which is about 40% of that used by the previous control law. The normal and tangential forces acting on the stance leg end are within the allowed friction cone with coefficient of friction $\mu < 0.7$; the maximum normal force is now less than 400 N. Fig. 17 displays the coordinates z_2 (vertical height of the end of the swing leg) and z_H (vertical height of the hips) for later comparison when walking on a compliant surface. Fig. 18 displays the absolute values of the actuator angular velocities versus the absolute values of torque (these values take into account the gear ratio) and shows that the results are compatible with RABBIT's actuators [6], [7]. Fig. 19 shows that the biped's motion converges to a limit cycle, as shown in the simulations.

VII. A Partial Robustness Evaluation

Robustness of the "optimal" controller of Section VI is investigated through simulation in three different situations: an external force acting on the hips or the torso; a change in the height of the walking surface; and walking on a compliant surface. The last point is studied separately since it necessitates a change in the model of the robot from the previous one: the compliance in the walking surface exercises all seven DOF of the model.

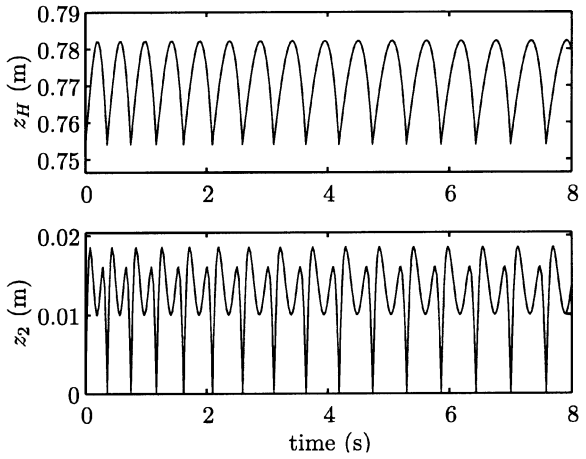

Fig. 17. Optimal trajectories. Plot of z_H and z_2 a (in meters).

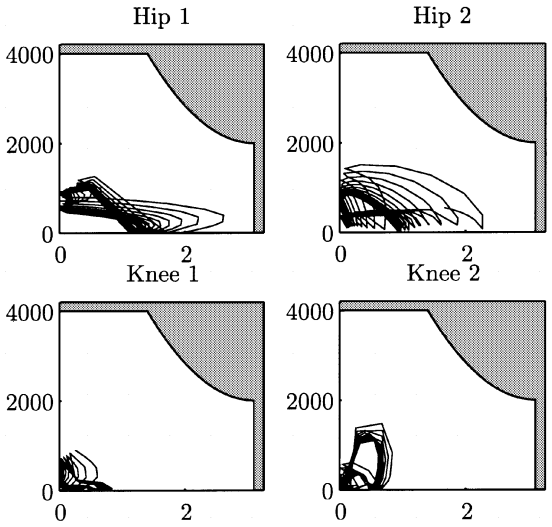

Fig. 18. Optimal trajectories. Plot of absolute value of actuator angular velocities (revolutions per minute) versus absolute value of actuator torques (in Newton meters); allowed region is in white.

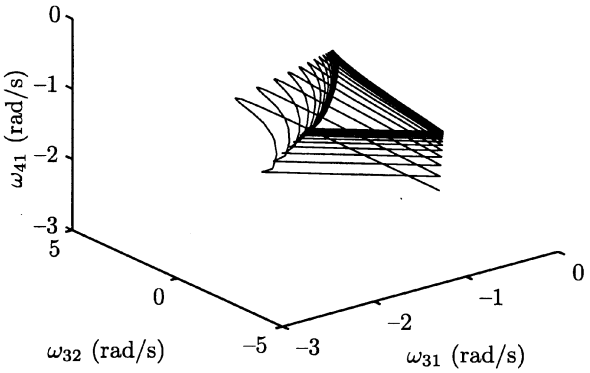

Fig. 19. Optimal trajectories. Three-dimensional projection of the attractive orbit. The straight-line segment of the trajectory (lower right) reflects the instantaneous change in velocity at the impact. The initial condition is in the lower right corner.

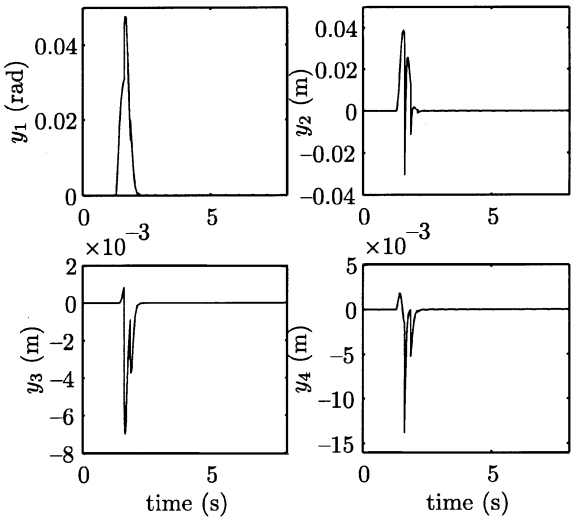

Fig. 20. Perturbation force. Plot of outputs versus time in the case of an external force acting on the torso.

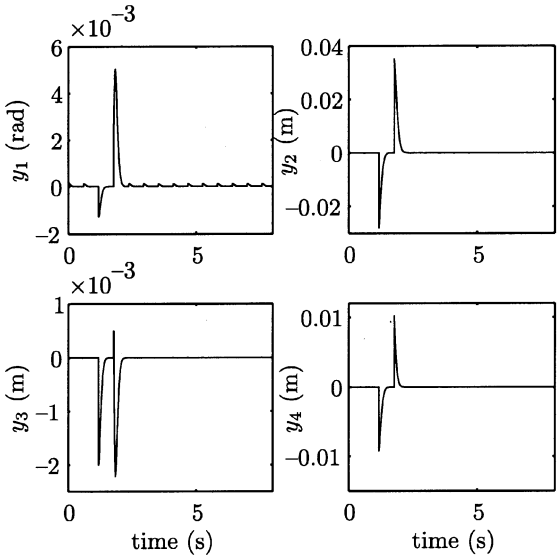

Fig. 21. Obstacle. Plot of outputs versus in the case of an obstacle on the ground.

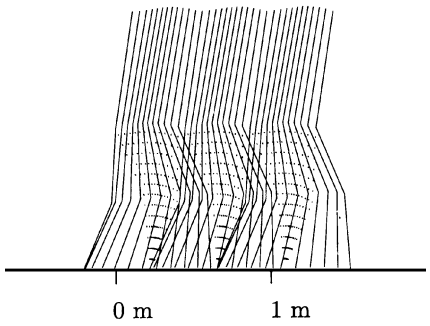

Fig. 22. Compliant surface. Plot of walking as a sequence of stick figures for the compliant surface.

A. External Perturbations

This subsection provides two results toward checking the robustness of the controller Section VI to external disturbances. In each case, the simulations have been performed with the controller parameters used previously, i.e., $\epsilon = 0.1$ and $\alpha = 0.9$. Furthermore, the initial velocity of the hips v_H^- has been taken to be 1.1 m/s (v_H^- is set to the value corresponding to the limit cycle). In order to limit the number of figures, only the output behavior is shown for theses tests. These plots, which give a good picture of the stability, are used to show whether the closed-loop system returns to the limit cycle after the perturbation is removed.

- External force. A horizontal force is applied in the middle of the torso at $t = 1.3$ s; its magnitude is 100 N, and its duration is 0.4 s. As borne out by Fig. 20, the system returns to the limit cycle when the force is removed. The test was also repeated, with similar results, with a force acting on the hips.
- Change in walking surface height. A 5-mm high obstacle[18] is placed on the walking surface in the path of the robot. Stepping on the obstacle introduces an error in the zero-altitude for two successive contacts (i.e., over two steps). When the biped steps up on the obstacle there is contact at $z_2 = 5$ mm, and when it steps off the obstacle, there is contact at $z_2 = -5$ mm. Fig. 21 shows that the controller takes this perturbation in stride.

B. Walking on a Compliant Surface

On the actual prototype, the contact between the ends of the legs and the ground will not be rigid and the ends of the legs may slip. This section presents the results of evaluating the controller (15) with the outputs defined in Section VI on a detailed simulator for RABBIT[19] that includes the normal forces on the legs due to a compliant contact with the ground [5], [20], [29] and the tangential forces due to dynamic friction [4], [28], [38]. For the sake of completeness, the nominal models of [4], [5], [18], [20], [28], [29], [38] are first summarized, a modification is discussed, and then the simulation results are reported.

The rigid and compliant models are conceptually very different. As presented in Section II, the rigid model is composed of a dynamical nonlinear system for the swing phase, and an impulsional system for the contact event. With the assumptions stated in Section II (in particular, the impact is instantaneous), this implies that there is no double support phase during a step. The compliant model, on the other hand, (see Fig. 22) is an ordinary (nonhybrid) dynamical nonlinear system and allows a double support phase where there is simultaneous contact between the swing leg and the ground and the stance leg and the ground. Of course, this fact was not taken into account in the synthesis of the controller, and applying the controller to the case of walking on a compliant surface allows a check of its robustness properties.

[18]This perturbation is not negligible in view of the value of the maximum height of the swing leg end z_2 (see Fig. 17) in the nominal case.

[19][Online.] Available: http://www-lag.ensieg.inpg/fr/recherche/cser/PRC-Bipedes/Prototype/rabbit.html

1) Compliant Contact and Friction Models: The dynamic model is based on the full seven DOF model of the biped with a computation of the forces acting on the end of each leg

$$D(q_e)\ddot{q_e} + C(q_e, \dot{q_e})\dot{q_e} + G(q_e) = Bu + J'(q_e)F \qquad (33)$$

where $q_e = (q_{31}, q_{32}, q_{41}, q_{42}, q_1, x_H, z_H)'$, $J(q_e)$ is the 4×7 Jacobian matrix of the end points of the two legs

$$J(q_e) = \frac{\partial}{\partial q_e}\begin{bmatrix} x_1(q_e) \\ z_1(q_e) \\ x_2(q_e) \\ z_2(q_e) \end{bmatrix} \qquad (34)$$

and F consists of the normal and tangential forces acting on the ends of the two legs $F = (F_{n1}\ F_{t1}\ F_{n2}\ F_{t2})'$. The robot's dynamics are then described by ordinary (nonhybrid) differential equations over the entire step, even during the impact, which will have a nonzero duration. Whenever one or both of the ends of the legs are in contact with ground, the resulting normal and tangential forces acting on the end of the leg are given by (if the penetration depth $z_G \leq 0$, i.e., the foot is touching the ground; if $z_G > 0$, these forces equal zero)

$$F_n = -\lambda_v^a |z_G|^n \dot{z}_G + k|z_G|^n, \quad F_t = \mu(d, v)|F_n|$$
$$\dot{d} = v - |v|\frac{\sigma_{h0}}{\alpha_{h0}}d, \quad \mu(d, v) = \sigma_{h0}d + \sigma_{h1}\dot{d} + \alpha_{h2}v$$

The model comes from a mathematical and physical analysis of the contact between a steel ball and a planar steel surface.[20] The model of the normal force can be viewed as a vertical nonlinear spring-damper; z_G is the penetration of the link into the ground, λ_v^a is the damping coefficient of the vertical damper, k_v the stiffness of the vertical spring and n is a coefficient characterizing the form of the surfaces in contact. For the biped robot, it is assumed that a sphere is impacting a Hertzian plane, so that $n = 1.5$ (this value corresponds to the contact of a steel ball and a planar steel surface, which is an approximation for the biped).

The tangential force, $F_t = \mu(d, v) \cdot |F_n|$, is in the form of a friction model with a nonconstant coefficient of friction. The LuGre friction model is used to evaluate the friction coefficient μ [4], [38]. This model supposes that the interface between the two contacting surfaces is a contact between bristles. The bristle dynamics are modeled by horizontal springs and dampers, which, if the applied tangential force is sufficient, are deflecting and slipping. The model uses the average deflection d of the bristles as the internal state of the friction, $\dot{d} = v - |v| \cdot (\sigma_{h0}/\alpha_{h0}) \cdot d$, where v is the relative velocity of the contacting surfaces, σ_{h0} the stiffness of the horizontal spring and α_{h0} is the coefficient of static friction. In the overall friction coefficient, $\mu(d) = \sigma_{h0} \cdot d + \sigma_{h1} \cdot \dot{d} + \alpha_{h2} \cdot v$, σ_{h1} is the damping coefficient of the horizontal damper, and α_{h2} is the coefficient of viscous friction.

In the case of the biped, the penetration z_{Gi} (where i equals 1 or 2) is the vertical coordinate of the end of leg i; this value is derived from the height of the hips z_H and the angular coordinates q_{3i} and q_{4i}, $z_{Gi} = z_H + L_3 \cdot \cos(q_{3i}) + L_4 \cdot \cos(q_{4i})$. The relative velocity v_i (where i equals 1 or 2) is the relative velocity of the end of the leg i with respect to the ground; this value is derived from the horizontal velocity of the hips $\dot{x}_H$, and the angular coordinates and velocities q_{3i}, q_{4i}, $\dot{q}_{3i}$ and $\dot{q}_{4i}$, $v_i = \dot{x}_H - L_3 \cdot \cos(q_{3i}) \cdot \dot{q}_{3i} - L_4 \cdot \cos(q_{4i}) \cdot \dot{q}_{4i}$.

[20]This is a rough approximation for the prototype because the wheel is made of polymer, resulting in less stiffness, a larger contact surface, and damping.

2) A Modification: The above model performs well when the walking surface is relatively compliant (ground penetration of on the order of a tens of millimeters). However, when the parameters are tuned up for a surface where the penetration of the leg is on the order of a few millimeters, it is difficult to adjust the damping to avoid ringing. For this reason, signed-square root terms were added to the normal force and the friction coefficient, as shown below, to provide better damping. Also, the magnitude of the friction coefficient μ was saturated at 0.7 to ensure that the leg could slip

$$\begin{cases} F_n = -\lambda_v^a \cdot |z_G|^n \cdot \dot{z}_G \\ \qquad -\lambda_v^b |z_G|^n \mathrm{sgn}(\dot{z}_G)\sqrt{|\dot{z}_G|} + k \cdot |z_G|^n \\ F_t = \mu(d, v) \cdot |F_n| \end{cases}$$
$$\begin{cases} \dot{d} = v - |v| \cdot \dfrac{\sigma_{h0}}{\alpha_{h0}} \cdot d \\ \mu(d, v) = \sigma_{h0} \cdot d + \sigma_{h1} \cdot \dot{d} + \alpha_{h2} \cdot v + \alpha_{h3}\mathrm{sgn}(\dot{v})\sqrt{|v|}. \end{cases} \qquad (35)$$

3) Simulations: In this section, the feedback controller of Section III-B with the outputs defined in Section VI (optimal trajectories) is directly applied to the biped robot model derived from (33), with the forces on the feet computed by (35). It is assumed that the mechanical parameters defined in Section IV are the same, and that the parameters of the controller have not been changed ($\alpha = 0.9$ and $\epsilon = 0.1$). The initial condition v_H^- is 1.1 m/s, i.e., the velocity corresponding to the limit cycle in the rigid case. The ground parameters are taken to be as close as possible to the parameters of the ground used by the prototype RABBIT

$$\lambda_v^a = 1.5 \times 10^6, \quad \lambda_v^b = 3 \times 10^4, \quad n = 1.5$$
$$k = 5 \times 10^5, \quad \sigma_{h0} = 260, \quad \sigma_{h1} = 0.6$$
$$\alpha_{h0} = 0.285, \quad \alpha_{h2} = 0.18, \quad \alpha_{h3} = 0.3.$$

Note that

1) $n = 1.5$ since the end of each of RABBIT's legs is equipped with a wheel in the frontal plane,
2) The stiffness parameter of the walking surface, k, was adjusted for a nominal penetration of approximately 7 mm. The damping coefficients were adjusted to yield minimal ringing.

In the case of the compliant contact model, there is a continuous change in the forces applied to the two legs, and hence there is not a contact moment, since, in fact, there is a nonzero period of time where both legs are in contact with the ground. However, to apply the controller computed on the basis of the rigid contact model, a contact moment must be declared so that the correct torques can be applied to the support leg and the swing leg. For the controller, therefore, contact was declared when the heights of the two feet were equal. This, of course, is exactly the same criterion as in the rigid contact model.

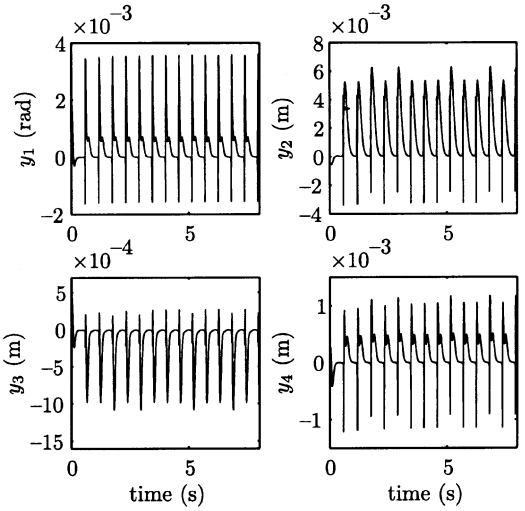

Fig. 23. Compliant surface. Plot of outputs used to define the controller versus time.

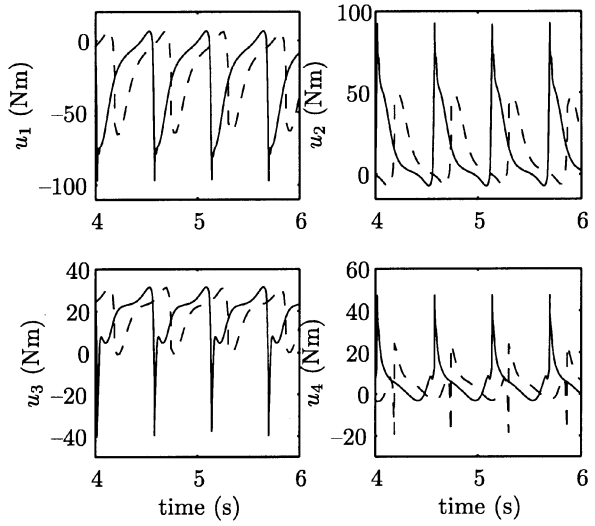

Fig. 24. Compliant surface. Plot of applied torques (in Newton meters) versus time in the compliant case (solid line) and, for reference, the rigid case (dashed line). The relative phasing has been deliberately offset for ease of reading the plot.

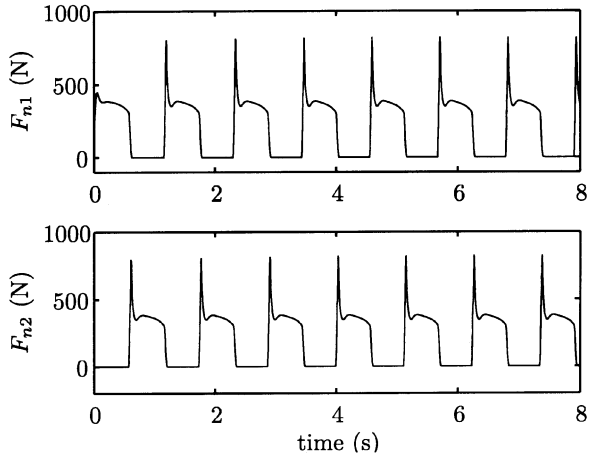

Fig. 25. Compliant surface. Plot of normal forces (in Newtons) acting on the stance leg end (top) and the swing leg end (bottom), versus time. For Figs. 25 and 26, Leg 1 (resp. 2) is not considered always as the stance (resp. swing) leg, but is acting as a normal leg, i.e., swapping between the stance and swing states during walking.

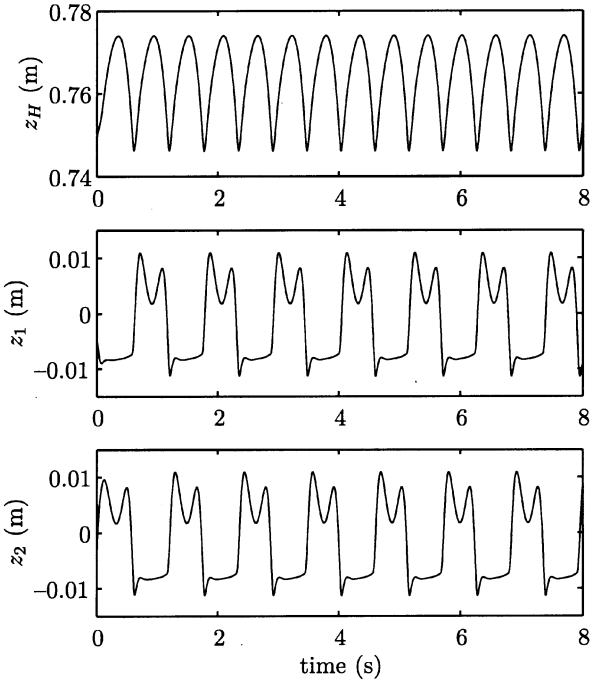

Fig. 26. Compliant surface. Plots of z_H, z_1, and z_2 (in meters) versus time.

The controller of Section III-B when applied to the model that includes the compliant walking surface results in an apparently attractive orbit. Figs. 23–26 present some simulation results over a few cycles near the stable orbit. Fig. 23 displays the outputs, which are still driven to zero before the impact. Fig. 24 displays the applied torques over a few walking cycles in the compliant (plain line) and rigid (dotted line) case; the peak torque magnitude is around 100 Nm in the compliant case. The average walking speed of the robot on the compliant surface equals about 0.6 m/s and is lower than in the rigid case: there seems to be additional loss of energy during the compliant impact, which induces a lower average walking speed. The torque at the impact has significantly increased, but otherwise throughout the step, the torques in the rigid and compliant cases are quite similar. Fig. 25 displays the normal forces acting on the leg ends: it is clear that there is a double support phase. Note also that the maximum values (about 800 N) are acceptable by the prototype RABBIT. Fig. 26 displays the coordinates z_H, z_1, and z_2, which give the vertical position of the hips and the ends of the legs. z_1 and z_2 become negative, showing that there is penetration in the ground of about 7 mm.

VIII. Conclusions

A rigorous stability analysis has been accomplished for a planar, five-link, four-actuator biped model when walking on a rigid, flat surface. The studied biped consists of a torso and two identical legs with revolute knees but no feet. It is thus under actuated during single support, as opposed to fully actuated (a control at each joint and the contact point with the ground). The

double support phase was modeled as being instantaneous, thus a walking motion cannot in any sense be construed as statically stable.

A steady walking cycle is a nontrivial periodic motion. This means that standard stability tools for static equilibria do not apply. Instead, one must use tools appropriate for the study of periodic orbits, such as Poincaré return maps. It is of course well known how to use numerical methods to compute a Poincaré return map and to find fixed points of it. The drawback in such a direct approach for bipeds is that it involves the numerical computation of a high-dimensional, nonlinear map and does not yield much insight for feedback design and synthesis.

A key development in [14] showed how to design a continuous-time control strategy in such a way that the existence and stability properties of periodic orbits can be checked, with necessary and sufficient conditions, on the basis of a one-dimensional map. This method was fully illustrated here on the five-link biped model. These results are a first attempt at a complete closed-loop stability analysis of a biped walker of nontrivial complexity. It is hoped that this analysis will inspire other researchers to develop additional analytically-oriented design methods for bipedal walkers.

The stability analysis performed here assumed a rigid contact model and instantaneous double support phase. In the biped robotics community, these assumptions have been generally regarded as being good approximations to walking on a stiff, though compliant, walking surface. To further investigate these two assumptions, a more complete model was used that included differential equations to compute the normal forces on the legs due to a compliant contact with the ground [5], [20], [29] and the tangential forces due to dynamic friction [4], [28], [38]. This model necessarily exercised the full seven DOF of the biped since the support leg is no longer assumed to act as a pivot. Furthermore, the walking motion necessarily has a nontrivial double support phase. Nevertheless, when the parameters in the compliant contact model were adjusted to correspond to walking on a relatively stiff surface, simulations showed that the controller designed under the simplifying assumptions of a rigid contact and instantaneous double support phase resulted in an apparently attractive limit cycle.

Currently, work is being done to more directly incorporate optimality into the feedback design process. An indirect method was illustrated in Section VI. The objective is to achieve stable walking motions that exploit the "natural" dynamics of the system. In this regard, it may also be interesting to "relax" somewhat the control laws used in this paper by moving away from the finite-time convergence properties, while still preserving the spirit of the simple and elegant analytical results used here. It seems that this might be possible by introducing a one-parameter family of controllers where the finite-time convergence property is only obtained as a limiting value of the parameter. This may involve a singular perturbation-like analysis of the hybrid robot model, that, if done carefully, may be able to approximately factor the Poincaré return map of the full-order closed-loop robot model into a portion that corresponds to the restricted Poincaré map and a portion corresponding to the "transversal" variables specified by h and $L_f h$. If the transversal variables are sufficiently rapidly contracting, then the restricted Poincaré map will still determine stability, just as in the "slow-fast" decomposition of a singularly perturbed system.

When the prototype is ready for testing, a number of implementation related issues will be investigated. These include: a nonlinear model of the gear boxes; potential compliance in the torque transmission path and links; effects of implementing the controller in discrete time; effects in errors in determining the impact condition. Experiments will be posted online at http://www-lag.ensieg.inpg/fr/recherche/cser/PRC-Bipedes/Prototype/rabbit.html as they are completed.

ACKNOWLEDGMENT

F. Plestan and G. Abba thank the French Research Group, Groupe de Recherche Commande de Robots à Pattes.

REFERENCES

[1] D. D. Bainov and P. S. Simeonov, *Systems With Impulse Effects: Stability, Theory and Applications*. Chichester, U. K.: Ellis Horwood, 1989.

[2] S. P. Bhat and D. S. Bernstein, "Continuous finite-time stabilization of the translational and rotational double integrators," *IEEE Trans. Automat. Contr.*, vol. 43, pp. 678–682, May 1998.

[3] W. M. Boothby, *An Introduction to Differentiable Manifolds and Riemannian Geometry*. New York: Academic, 1975.

[4] C. Canudas, H. Olsson, K. J. Aström, and P. Lischinsky, "A new model for control of systems with friction," *IEEE Trans. Automat. Contr.*, vol. 40, pp. 419–425, Mar. 1995.

[5] C. Canudas, L. Roussel, and A. Goswani, "Periodic stabilization of a 1-DOF hopping robot on nonlinear compliant surface," in *Proc. IFAC Symp. Robot Control*, Nantes, France, Sept. 1997, pp. 405–410.

[6] C. Chevallereau and Y. Aoustin, "Optimal reference trajectories for walking and running of a biped robot," *Robotica*, vol. 19, pp. 557–569, 2001.

[7] C. Chevallereau and P. Sardain, "Design and actuation optimization of a 4-axes biped robot for walking and running," in *Proc. IEEE Int. Conf. Robotics and Automation*, San Francisco, CA, Apr. 2000, pp. 3365–3370.

[8] J. J. Eng, D. A. Winter, and A. E. Patla, "Strategies for recovery from a trip in early and late swing during human walking," *Exp. Brain Res.*, vol. 102, no. 2, pp. 339–349, 1994.

[9] ——, "Intralimb dynamics simplify reactive control strategies during locomotion," *J. Biomech.*, vol. 30, no. 5, pp. 581–588, 1997.

[10] C. François and C. Samson, "A new approach to the control of the planar one-legged hopper," *Int. J. Robot. Res.*, vol. 17, no. 11, pp. 1150–1166, 1998.

[11] Y. Fujimoto and A. Kawamura, "Simulation of an autonomous biped walking robot including environmental force interaction," *IEEE Robot. Automat. Mag.*, pp. 33–42, June 1998.

[12] F. Ghorbel and M. W. Spong, "Integral manifolds of singularly perturbed systems with application to rigid-link flexible-joint multibody systems," *Int. J. Non-Linear Mech.*, vol. 34, pp. 133–155, 2000.

[13] A. Goswani, B. Espiau, and A. Keramane, "Limit cycles and their stability in a passive bipedal gait," in *Proc. IEEE Int. Conf. Robotics and Automation*, Minneapolis, MN, Apr. 1996, pp. 246–251.

[14] J. W. Grizzle, G. Abba, and F. Plestan, "Asymptotically stable walking for biped robots: analysis via systems with impulse effects," *IEEE Trans. Automat. Contr.*, vol. 46, pp. 51–64, Jan. 2001.

[15] ——, "Proving asymptotic stability of a walking cycle for a five-DOF biped robot model," in *Proc. Int. Conf. Climbing and Walking Robots*, Portsmouth, U. K., 1999, pp. 69–81.

[16] J. Guckenheimer and P. Holmes, *Nonlinear Oscillations, Dynamical Systems, and Bifurcations of Vector Fields*. New York: Springer-Verlag, 1996, vol. 42, Applied Mathematical Sciences.

[17] G. W. Howell and J. Baillieul, "Simple controllable walking mechanisms which exhibit bifurcations," in *Proc. IEEE Conf. Decision and Control*, vol. 3, 1998, pp. 3027–3032.

[18] R. H. A. Hensen, M. J. G. van de Molengraft, and M. Steinbuch, "Frequency domain idenitification of dynamic friction model parameters," *IEEE Trans. Automat. Contr.*, vol. 10, pp. 191–196, Feb. 2002.

[19] Q. Huang, K. Yokoi, S. Kajita, K. Kaneko, H. Arai, N. Koyachi, and K. Tanie, "Planning walking patterns for a biped robot," *IEEE Trans. Robot. Automat.*, vol. 17, pp. 280–289, June 2001.
[20] K. H. Hunt and F. R. Crosseley, "Coefficient of restitution interpreted as damping in vibroimpact," *J. Appl. Mech.*, pp. 440–445, 1975.
[21] Y. Hurmuzlu and D. B. Marghitu, "Rigid body collisions of planar kinematic chains with multiple contact points," *Int. J. Robot. Res.*, vol. 13, no. 1, pp. 82–92, 1994.
[22] A. Isidori, *Nonlinear Control Systems: An Introduction*, 2nd ed. Berlin, Germany: Springer-Verlag, 1989.
[23] D. D. Koditschek and M. Buhler, "Analysis of a simplified hopping robot," *Int. J. Robot. Res.*, vol. 10, no. 6, pp. 587–605, 1991.
[24] P. Kokotovic, H. K. Khalil, and J. O'Reilly, *Singular Perturbation Methods in Control: Analysis and Design*. London, U. K.: Academic, 1986.
[25] A. D. Kuo, "Stabilization of lateral motion in passive dynamic walking," *Int. J. Robot. Res.*, vol. 18, no. 9, pp. 917–930, 1999.
[26] M. de Lasa and M. Buehler, "Dynamic compliant walking of a quadruped robot: preliminary experiments," in *Proc. Int. Conf. Climbing and Walking Robots*, Madrid, Spain, 2000, pp. 153–160.
[27] H. Lim and A. Takanishi, "Walking pattern generation for biped locomotion," in *Proc. Int. Symp. Robotics*, Seoul, Korea, Apr. 2001, pp. 1551–1556.
[28] P. A. Lischinsky, "Compensation de Frottement et Commande en Position d'un Robot Hydraulique Industriel," Ph.D. dissertation (in French), Inst. Nat. Polytechnique de Grenoble, Grenoble, France, 1997.
[29] D. W. Marhefka and D. E. Orin, "Simulation of contact using a nonlinear damping model," in *Proc. IEEE Int. Conf. Robotics and Automation*, Minneapolis, MN, Apr. 1996, pp. 1662–1668.
[30] K. Ono, R. Takahashi, and T. Shimada, "Self-excited walking of a biped mechanism," *Int. J. Robot. Res.*, to be published.
[31] K. Ono, K. Yamamoto, and A. Imadu, "Control of giant swing motion of a two-link horizontal bar gymnast robot," *Adv. Robot.*, vol. 15, no. 4, pp. 449–465, 2001.
[32] T. S. Parker and L. O. Chua, *Practical Numerical Algorithms for Chaotic Systems*. New York: Springer-Verlag, 1989.
[33] F. Pfeiffer, K. Loffler, and M. Gienger, "The concept of jogging JOHNNIE," in *Proc. IEEE Int. Conf. Robotics and Automation*, Washington, DC, May 2002, pp. 3129–3135.
[34] J. Pratt, P. Dilworth, and G. Pratt, "Virtual model control of a bipedal walking robot," in *Proc. IEEE Int. Conf. Robotics and Automation*, Albuquerque, NM, Apr. 1997, pp. 183–196.
[35] J. Pratt and G. Pratt, "Intuitive control of a planar bipedal walking robot," in *Proc. IEEE Int. Conf. Robotics and Automation*, Leuven, Belgium, May 1998, pp. 201–202.
[36] G. Pratt, "Legged robots at MIT: what's new since Raibert?," *IEEE Robot. Automat. Mag.*, pp. 5–10, Sept. 2000.
[37] M. Reyhanoglu, A. van der Schaft, N. H. McClamroch, and I. Kolmanovsky, "Dynamics and control of a class of underactuated mechanical systems," *IEEE Trans. Automat. Contr.*, vol. 44, pp. 1663–1671, Sept. 1999.
[38] L. Roussel, "Génération de Trajectoires de Marche Optimales Pour un Robot Bipède," Ph.D. dissertation (in French), Inst. Nat. Polytechnique de Grenoble, Grenoble, France, 1998.
[39] M. H. Raibert, "Legged robots," *Commun. ACM*, vol. 29, no. 6, pp. 499–514, 1986.
[40] ——, *Legged Robots That Balance*. Cambridge, MA: MIT Press, 1986.
[41] U. Saranli, W. J. Schwind, and D. T. Kodistschek, "Toward the control of multi-joined, monopod runner," in *Proc. IEEE Int. Conf. Robotics and Automation*, Leuven, Belgium, May 1998, pp. 2676–2682.
[42] M. W. Spong, "Passivity-based control of the compass gait biped," in *Proc. IFAC World Congress*, vol. B, Beijing, China, July 1999, pp. 19–23.
[43] M. W. Spong and M. Vidyasagar, *Robot Dynamics and Control*. New York: Wiley, 1991.
[44] A. Takanishi, "Humanoid robots and animal robots—toward entertainment robot market in 21st century," in *Proc. Int. Symp. Robotics*, Seoul, Korea, Apr. 2001, pp. 2–7.
[45] B. Thuilot, A. Goswani, and B. Espiau, "Bifurcation and chaos in a simple passive bipedal gait," in *Proc. IEEE Int. Conf. Robotics and Automation*, Albuquerque, NM, Apr. 1997, pp. 792–798.
[46] M. Vukobratovic, B. Borovac, D. Surla, and D. Stokic, *Biped Locomotion*. Berlin, Germany: Springer-Verlag, 1990.
[47] J. Yamaguchi, D. Nishino, and A. Takanishi, "Realization of dynamic biped walking varying joint stiffness using antagonistic driven joints," in *Proc. IEEE Int. Conf. Robotics and Automation*, Leuven, Belgium, May 1998, pp. 2022–2029.
[48] H. Ye, A. N. Michel, and L. Hou, "Stability theory for hybrid dynamical systems," *IEEE Trans. Automat. Contr.*, vol. 43, pp. 461–474, Apr. 1998.
[49] K. Y. Yi, "Walking of a biped robot with compliant ankle joints: implementation with KUBCA," in *Proc. IEEE Conf. Decision and Control*, Sydney, Australia, Dec. 2000, pp. 4809–4814.

Franck Plestan (M'99–A'00) received the Ph.D. degree in automatic control from the Ecole Centrale de Nantes, Nantes, France, in 1995.

From September 1996 to August 2000, he was with the Université Louis Pasteur, Strasbourg, France. In September 2000, he joined the Ecole Centrale de Nantes, Nantes, France, where he is currently Assistant Professor. His research interests include nonlinear control, theoretical aspects of nonlinear observer design and control of electromechanical and mechanical systems.

Dr. Plestan received the 2002 George S. Axelby award for the best paper [14] published in the IEEE TRANSACTIONS ON AUTOMATIC CONTROL during the years 2000 and 2001.

Jessy W. Grizzle (S'78–M'79–SM'90–F'97) received the Ph.D. degree in electrical engineering from The University of Texas at Austin in 1983.

Since September 1987, he has been with The University of Michigan, Ann Arbor, where he is a Professor of Electrical Engineering and Computer Science. His research interests lie in the theory and practice of nonlinear control. He has been a consultant in the automotive industry since 1986, where he jointly holds over a dozen patents dealing with emissions reduction through improved control system design. He is currently an Associate Editor for *Automatica*, and a past Associate Editor for *Systems & Control Letters*.

Dr. Grizzle is a past Associate Editor of the IEEE TRANSACTIONS ON AUTOMATIC CONTROL. He served as Publications Chairman for the 1989 CDC, and from 1997 through 1999 served on the Control Systems Society's Board of Governors. He was a NATO Postdoctoral Fellow from January to December 1984; he received an NSF Presidential Young Investigator Award in 1987, the Paper of the Year Award from the IEEE Vehicular Technology Society in 1993, the University of Michigan's Henry Russell Award for outstanding research in 1993, a College of Engineering Teaching Award in 1993, and received the 2002 George S. Axelby award for the best paper [14] published in the IEEE TRANSACTIONS ON AUTOMATIC CONTROL during the years 2000 and 2001.

Eric R. Westervelt (S'97) received the B.S. degree in computer and systems engineering from Rensselaer Polytechnic Institute, Troy, NY in 1997 and the M.S. degree in electrical engineering in 1999 from the University of Michigan, Ann Arbor, where he is currently working toward the Ph.D. degree.

From 1998 to 1999, he was an intern at the Hirata Corporation, a robotics firm, in Kumamoto, Japan.

Gabriel Abba (M'99) joined the Ecole Normale Supérieure de Cachan, France, in 1979, and received the "agrégation" from the Ministry of Education in electrical engineering in 1982. He received the Doctorate degree in electronics and robotics from the University of Paris XI-Orsay, Paris, France, in 1986.

Since 1999, he has been Professor at the University of Metz, Metz, France. He is the head of Industrial Systems and Maintenance Department and the head of Mechanical Production Laboratory. His research interests include development, modeling and control of robots, especially control of legged robots, visual servoing, and control of high-speed drives and spindle for industrial applications.